GE Nuclear Energy

General Electric Company
175 Curtner Avenue, San Jose CA 95125

GE-NE-0000-0007-2342-R1-NP
DRF 0000-0007-2342
Revision 1
Class I
July 2003

## Final Report

# Entergy Northeast Vermont Yankee Neutron Flux Evaluation

**Principal Contributor:**

Tang Wu

**Principal Verifiers:**

S. S. Wang
H. A. Careway

**Technical Projects Manager:**

David J. Robare

# IMPORTANT NOTICE REGARDING THE CONTENTS OF THIS REPORT

## Please Read Carefully

### A. Disclaimer

The only undertakings of the General Electric Company (GE) respecting information in this document are contained in the contract between the company receiving this document and GE. Nothing contained in this document shall be construed as changing the applicable contract. The use of this information by anyone other than a customer authorized by GE to have this document, or for any purpose other than that for which it is intended, is not authorized. With respect to any unauthorized use, GE makes no representation or warranty, and assumes no liability as to the completeness, accuracy or usefulness of the information contained in this document, or that its use may not infringe privately owned rights.

### B. Information Notice

This is a non-proprietary version of the document GE-NE-0000-0007-2342-R1-P, which has the proprietary information removed. Portions of the document that have been removed are indicated by an open and closed bracket as shown here [[ ]].

# TABLE OF CONTENTS

## LIST OF TABLES



## LIST OF FIGURES

## ACRONYMS AND ABBREVIATIONS

| | |
|---|---|
| BAF | Bottom of Active Fuel |
| BOC | Beginning of Cycle |
| ECP | Engineering Computer Program |
| EFPY | Effective Full-Power Years |
| ENDF | Evaluated Nuclear Data File |
| ENVY | Entergy Northeast Vermont Yankee |
| EOC | End of Cycle |
| GE | General Electric |
| GE-NE | General Electric Nuclear Energy |
| GNF | Global Nuclear Fuel |
| IASCC | Irradiation Assisted Stress Corrosion Cracking |
| ID | Inside Diameter |
| LTR | Licensing Topical Report |
| MOC | Middle of Cycle |
| MWt | Megawatt Thermal |
| NRC | Nuclear Regulatory Commission |
| OD | Outside Diameter |
| ORNL | Oak Ridge National Laboratory |
| RG | Regulatory Guide |
| RPV | Reactor Pressure Vessel |

# 1.0 INTRODUCTION

Neutron irradiation of the reactor pressure vessel (RPV) causes reduction in material ductility and creates structural embrittlement at higher operating temperatures. The effect is particularly significant when impurities such as nickel, copper, or phosphorus are present in noticeable levels, as is commonly true for the RPV steel. Therefore determination of neutron fluence level is one of the first steps toward RPV fracture toughness evaluations.

Irradiation by fast neutrons (with energies greater than 1 MeV) can also be a concern with respect to irradiation assisted stress corrosion cracking (IASCC) for reactor internal components such as core shroud, top guide, core plate, etc. Crack growth evaluation for these components also requires adequate determination of neutron fluence level.

Neutron flux, or fluence rate, can be determined through radiochemical analysis of the surveillance flux wire samples; which are made of iron, copper, or nickel, sealed inside a capsule and held in place by a holder near the RPV inside surface. The calculated ratio of surveillance sample flux to the RPV peak flux defines a lead factor. This lead factor can be applied to the sample dosimetry data to determine the RPV peak flux.

Neutron flux can also be determined by solving the Boltzmann neutron transport equation with the discrete ordinates method or Monte Carlo simulation. When appropriate bias is applied to the calculation results, these numerical methods can be used to obtain the best-estimate flux distribution.

The first objective (Task 1) of this work is to evaluate the capsule flux and neutron flux distributions at the RPV and at the shroud for the period during which the last removed capsule was resident in the Entergy Northeast Vermont Yankee (ENVY) plant. The second objective (Task 2) is to evaluate the flux distributions at the RPV and at the shroud for a representative modern core to determine the impact of core and fuel design changes that have occurred since the capsule removal. Once the neutron flux is determined, the lifetime fluence can be determined by integrating the fluxes over the total irradiation period.

# 2.0 SUMMARY AND CONCLUSIONS

## 2.1 Methodology

The methodology used for the neutron flux calculation is documented in the GE's Licensing Topical Report (LTR) NEDC-32983P-A [1], which was approved by the U.S. NRC for licensing applications in the Safety Evaluation Report [2]. In general, GE's methodology described in the LTR adheres to the guidance in Regulatory Guide (RG) 1.190 [3] for neutron flux evaluation. In this evaluation, the fast neutron flux distribution is calculated based on the three-dimensional flux synthesis of two separate two-dimensional flux solution calculations performed in an (r,z) and an (r,θ) model. These flux solution calculations are performed using the two-dimensional discrete ordinates code DORTG01V, which is a controlled version of DORT in the GE Engineering Computation Program (ECP) library [4].

## 2.2 Neutron Flux for Cycles 9 and 8

Task 1 of this evaluation is based on the core data from Cycles 8 and 9, at the end of which the surveillance capsule was removed from the plant. The analysis inputs and core data have been provided by Entergy through concurrence and transmittals [5, 6]. The core power used is 1593 MWt.

The calculated peak fast flux (E>1 MeV) at the RPV inside surface is 2.97E8 n/cm$^2$-s for Cycle 9 and 2.70E8 n/cm$^2$-s for Cycle 8. The peak flux for the first quadrant is located at the azimuth of 0° and at the elevation of 92 and 96 inches above the bottom of the active fuel (BAF), respectively for Cycle 9 and Cycle 8. Fluxes for other quadrants are expected to be similar due to quadrant symmetry of the core design as well as the arrangement of vessel internal components.

[[

]]

The peak fast flux for the shroud inside surface (nominal ID) is 8.38E10 n/cm$^2$-s for Cycle 9 and 7.78E10 n/cm$^2$-s for Cycle 8. The peak flux for the first quadrant is located at the azimuth of 90° for Cycle 9 and 83° for Cycle 8. The peak elevation is 98 and 102 inches above the BAF, respectively for Cycle 9 and Cycle 8.

## 2.3 Neutron Flux for Modern Cores

Neutron flux for the ENVY modern core is evaluated based on Cycle 21 core data. The calculated peak fast flux at the RPV inside surface is 2.96E8 n/cm$^2$-s. The peak flux for the first quadrant is located at the azimuth of 0° and at the elevation of 84 inches above the BAF.

[[ ]]

The peak fast flux for the shroud inside surface (nominal ID) is 8.17E10 n/cm$^2$-s. The peak flux is located at the azimuth of 83°and the peak elevation is 89 inches above the BAF.

It is concluded that flux levels from Cycle 21 are comparable to the average values of Cycles 9 and 8. Thus, Cycle 21 fluxes can be used to provide a conservative estimate of the time-integrated neutron fluences over the plant life.

Assessment of impact on flux levels for Cycle 23, which contains fuel bundles with part-length rods in the core periphery, is also performed. Comparison of power density of the governing peripheral bundles between Cycle 23 and Cycle 21 indicates that Cycle 23 fluxes will be bounded by Cycle 21.

## 2.4 Neutron Fluence

Cycle 21 fluxes are used to provide a conservative estimate of the neutron fluences at the end of plant life of 32 and 54 EFPY. The peak 32-EFPY fluence is 2.99E17 n/cm$^2$ at the RPV inside surface and 8.25E19 n/cm$^2$ at the shroud inside surface. The peak 54-EFPY fluence is 5.04E17 n/cm$^2$ at the RPV inside surface and 1.39E20 n/cm$^2$ at the shroud inside surface. The axial distribution of the RPV fast neutron fluences indicates that the 32-EFPY fluence greater than 1.0E17 n/cm$^2$ is confined to the active fuel zone.

# 3.0 EVALUATION

## 3.1 Scope

Fast neutron fluxes in the beltline region extending from the core through the RPV are calculated in this analysis. Task 1 of this work is to evaluate the capsule flux and neutron flux distributions at the RPV and at the shroud for the period during which the last removed capsule was resident in the ENVY plant. Since the capsule was removed after shutdown on March 1983 (End of Cycle 9) [7], the core data that are important for this calculation are those of Cycle 9 and Cycle 8.

Task 2 of this work is to evaluate the flux distributions at the RPV and at the shroud for a representative modern core to determine the impact of core and fuel design changes that have occurred since the capsule removal. This flux evaluation will be based on the Cycle 21 core data, based on the agreement between GE and Entergy as part of the Design Input Request [5].

Once the neutron flux is determined, the neutron fluence at the end of plant life can be determined by integrating the fluxes over the irradiation time.

## 3.2 Inputs and Assumptions

The operating condition assumed for this analysis is based on the specific core design data of the cycles of interest. For the older cycles, core data have been provided by Entergy [6]. For the modern core, core data were retrieved and processed from GE's Engineering Data Bank. Core data that are pertinent to the flux calculations include core loading, bundle types, bundle heavy metal mass, and void fraction (or water density) and fuel exposure data. The currently licensed power is 1593 MWt.

The RPV and shroud dimensions, together with the configuration and location of surveillance capsule holder, are provided in Reference 6 and shown in Table 3-1.

## 3.3 Method of Evaluation

The methodology used for the neutron flux calculation is documented in a Licensing Topical Report (LTR) NEDC-32983P-A [1], which was approved by the U.S. NRC in the Safety Evaluation Report for referencing in licensing actions [2]. In general, GE's methodology described in the LTR adheres to the guidance in Regulatory Guide 1.190 [3] for neutron flux evaluation.

[[

]]

This synthesis approach is consistent with the GE approved methodology.

The flux calculations are performed with DORTG01V, which is a controlled version of DORT in the GE Engineering Computation Program (ECP) library [4]. The NRC has approved the use of DORT as part of the GE methodology [2].

The cross-section data used in the DORT calculation are processed with the nuclear cross-section processing package [Ref. 9] in the GE ECP. [[

]] A $P_3$ truncation of the Legendre polynomial expansion, which meets Regulatory Position 1.1.2 in RG 1.190, is used to approximate the anisotropy in the differential scattering cross sections. The approach discussed here is consistent with the approved LTR methodology.

The cross section library used in the GE ECP is based on Version V of the Evaluated Nuclear Data File (ENDF/B-V). However, cross sections for the important components of BWR neutron flux calculation - oxygen, hydrogen, and individual iron isotopes - have been upgraded to ENDF/B-VI to meet the guidelines of Regulatory Guide 1.190.

### 3.3.1 Core Loading

Cycle 21 is a modern core. The core load contained 220 bundles of GE13 and 148 bundles of GE9B. GE13 contains both full-length and part-length fuel rods. GE9B contains only full-length fuel rods. Fuel bundles in the outermost row contained only GE9B fuel bundles.

Cycle 9 core load contained 356 bundles of GE6 and 12 bundles of GE4. Fuel bundles in the outermost row were GE6 and GE4 [Ref. 6].

Cycle 8 core load contained 236 bundles of GE6 and 132 bundles of GE4 at various enrichment. Fuel bundles in the outermost row were all GE4 [Ref. 6].

### 3.3.2 (R,θ) Model

Figure 3-1 shows a quadrant of the core and the vessel internal components that are relevant to the flux calculation. [[

]]

The (r,θ) analysis used the polar coordinates to define the calculation model as a planar sector between reactor azimuths 0° and 90°. [[

]]

ENVY installed the shroud restraint tie rods during the 1996 Refueling Outage [Ref. 5]. These tie rods have been present since the beginning of Cycle 19. These rods have an outer diameter of 4 inches and were placed at the radial location of 3.625 inches from the inner vessel wall in each of the 45°, 135°, 225°, and 315° azimuths. These tie rods were modeled as homogenized cylinder, with a steel area fraction of 93%.

In the angular coordinate θ, the mesh size is ½ degree per mesh interval, except for the two boundary nodes, which is ¼ degree. For a core quadrant, a total of 181 fine meshes are used in the θ-direction. This model is more detailed than the minimum requirement of 40 intervals per octant stipulated in Section 1.3.1. of RG 1.190.

Radial meshes vary in sizes. Generally, a fine mesh is provided near material interfaces, where significant flux gradients are expected. Fine meshes are also applied near the shroud and the capsule. Sufficient fine mesh steps are provided to simulate the outer boundary profiles of the core. The mesh step is fine enough such that the actual core boundary can be approximated to the nearest 0.8 cm. [[

]]

The (r,θ) calculation is performed for the first quadrant of the reactor. The model includes three sets of jet-pump/riser, which are centered at 30°, 60°, and 90°. It also includes the 30° capsule, which is completely shadowed by the jet-pump riser, and the shroud restraint tie rod at 45° for the modern cores. The azimuthal distribution of RPV flux in the first quadrant is expected to be representative of other quadrants because of the quadrant symmetry in the power distribution. The RPV flux at 0 and 180 degrees is expected to be higher than that at 90 and 270 degrees, due to the absence of jet pumps.

### 3.3.3 (R,Z) Model

[[

]]

### 3.3.4 Material Composition and Coolant Density

Material compositions in each calculation model are treated as homogeneous mixtures. The volume fractions of solid material in the three core regions are calculated based on specific fuel bundle design data. [[

]]

[[

]]

### 3.3.5 Neutron Source Distribution

The energy produced per fission and the neutron yield data that are representative of the cycle were obtained from TGBLA calculations. These data are then used to generate the total neutron source in the core. Spatial distribution of the neutron source density is simulated based on relative cycle-integrated energy production. [[

]]

Figures 3-3, 3-4, and 3-5 show the bundle-dependent relative cycle energy (normalized to the core average) at core midplane elevation (axial node 13) for Cycles 21, 9, and 8, respectively. These discrete data in the (x,y) plane are processed to form the neutron source distribution in the (r,θ) meshes for the (r,θ) calculation. The power densities of the peripheral bundles near the azimuth of the peak RPV or shroud fluxes have a direct impact on the shroud and RPV flux levels. [[

]]

## 3.4 Bias and Uncertainty

[[

]]

[1] These values are included in Section 4.4 and 5.4 for comparison purpose only. The bias and uncertainty associated with these values have not been assessed.

**Table 3-1 Design Input Data for Flux Calculation (Entergy Verified)**

| Parameter | Data (default unit is inch) | Reference Drawing |
|---|---|---|
| (A) Surveillance Capsule Basket | | |
| Thickness | 0.895 | 117C4335P1 |
| Width | 7.06 max | 117C4335P1 |
| Length | 13.275 | 117C4335P1, 129B3157P1 |
| Azimuths, degrees | 30, 120, 300 | 921D514 |
| Radial Position of Basket Center, from RPV Clad | 0.875 | 919D294, 129B3157P1 |
| Elevation of Basket Center, above BAF | 73.6975 | 919D294, 117C4335P1 |
| (B) RPV (Beltline) | | |
| RPV Base Metal ID | 205.25 | 104R940 |
| RPV Thickness | 5.064 | Figure 7 of Battelle Report BCL-585-84-3, May 15, 1984. |
| RPV Clad Thickness | 0.125 | UFSAR Rev.17 Section 4.2.4.1 |
| (C) Shroud (Active Fuel Region) | | |
| Shroud ID | 163.75 nom | 729E956 |
| Shroud Thickness | 1.75 | 729E956 |
| (D) Jet Pump Components | | |
| Recirc. Inlet Nozzles Azimuths, degrees | 30, 60, 90, 120, 150, 210, 240, 270, 300, 330 | 919D294 Sh 2 (VPF1842) |
| Jet Pump Riser Pipe | 10" Sch 40 | 719E113 |
| Jet Pump Inlet Mixer OD | 6.625 | 719E113 |
| Jet Pump Inlet Mixer ID | 6.07 | 920D278 |
| Radial Location of Riser from Core Center | 91.844 | 919D294 Sh 3 |

| Parameter | Data (default unit is inch) | Reference Drawing |
|---|---|---|
| Radial Offset, Mixer to Riser | 0.32 | 719E113 |
| Radial Location of Mixer from Core Center | 92.382 | Derived |
| Distance between Mixers, centerline to centerline | 25.125 | 919D294 Sh 3 |
| (E) Top Guide Beam | | |
| Upper Elevation | 370.25 | 104R940 |
| Lower Elevation | 358.75 | 104R940 |
| (F) Core Plate | | |
| Upper Elevation | 198.56 | 104R940 |
| Thickness | 2 | 729E957 |
| Elevation of top of core plate support flange | 184.56 | 104R940 |
| (G) Other Core Data | | |
| Thermal Power | 1593 MWt | UFSAR Rev.17 Table 3.7.1 |
| Elevation of Bottom of Active Fuel (BAF) | 207.5 | 104R940 |
| Density of Bypass Water between Shroud and Fuel Bundles | 0.738 g/cm$^3$ | Saturated water at $P_{sat}$=1025 psia, $T_{sat}$=547.56°F |
| Density of Downcomer Water | 0.760 g/cm$^3$ | Subcooled (20°F) water |

**Figure 3-1. Core Layout and Vessel Internal Components**

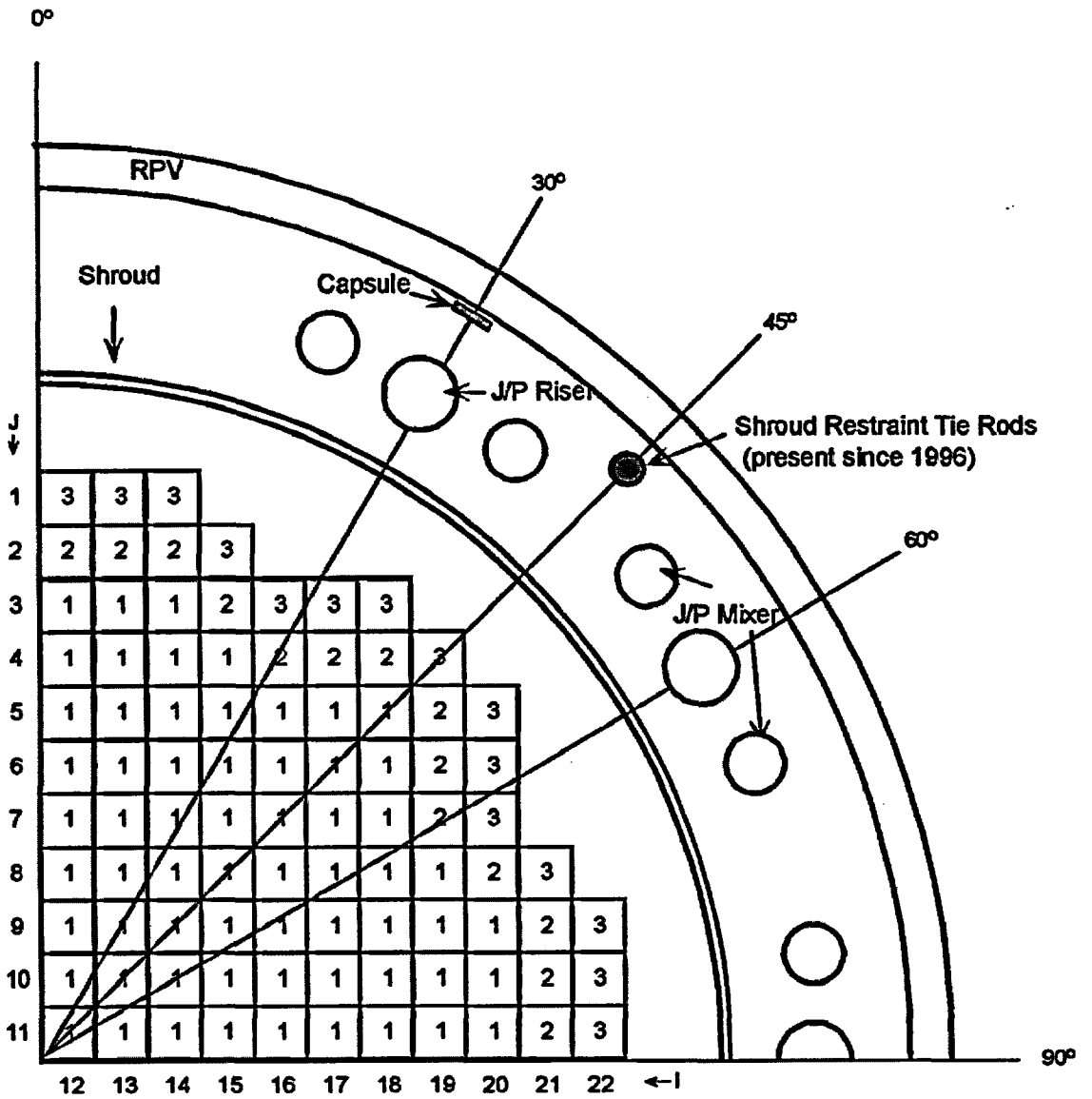

**Figure 3-2. Schematic of (R,Z) Model**

[[

]]

**Figure 3-3. Relative Energy by Bundle at Core Midplane – Cycle 21**

| J= \ I= | 12 | 13 | 14 | 15 | 16 | 17 | 18 | 19 | 20 | 21 | 22 |
|---|---|---|---|---|---|---|---|---|---|---|---|
| 1 | 0.6426 | 0.5524 | 0.4757 | | | | | | | | |
| 2 | 1.2613 | 1.1466 | 1.0266 | 0.6314 | | | | | | | |
| 3 | 1.3561 | 1.4504 | 1.2836 | 1.1501 | 0.7873 | 0.5657 | 0.4749 | | | | |
| 4 | 1.5451 | 1.1986 | 1.5154 | 1.3346 | 1.2106 | 1.0834 | 0.9354 | 0.5655 | | | |
| 5 | 1.2038 | 1.5989 | 1.4743 | 1.5755 | 1.3679 | 1.0216 | 1.1912 | 0.9381 | 0.4851 | | |
| 6 | 1.4851 | 1.2213 | 1.5996 | 1.2363 | 1.5448 | 1.3293 | 1.0256 | 1.0878 | 0.5703 | | |
| 7 | 1.1089 | 1.3433 | 1.1594 | 1.5079 | 1.1591 | 1.5525 | 1.3742 | 1.2161 | 0.8036 | | |
| 8 | 1.4337 | 1.1034 | 1.4656 | 1.3562 | 1.5263 | 1.2452 | 1.5811 | 1.3395 | 1.1524 | 0.6222 | |
| 9 | 1.1222 | 1.4330 | 1.1354 | 1.5151 | 1.2211 | 1.6216 | 1.4828 | 1.5188 | 1.2810 | 1.0254 | 0.5175 |
| 10 | 1.3532 | 1.1214 | 1.4522 | 1.1601 | 1.4033 | 1.2307 | 1.6013 | 1.1948 | 1.4466 | 1.1412 | 0.5471 |
| 11 | 1.1563 | 1.3571 | 1.1257 | 1.4710 | 1.1425 | 1.4773 | 1.1833 | 1.5352 | 1.3500 | 1.2553 | 0.6285 |

**Figure 3-4. Relative Energy by Bundle at Core Midplane – Cycle 9**

| J= \ I= | 12 | 13 | 14 | 15 | 16 | 17 | 18 | 19 | 20 | 21 | 22 |
|---|---|---|---|---|---|---|---|---|---|---|---|
| 1 | 0.6902 | 0.5300 | 0.4590 | | | | | | | | |
| 2 | 1.0230 | 0.9586 | 0.8842 | 0.5987 | | | | | | | |
| 3 | 1.1234 | 1.2056 | 1.0573 | 1.0488 | 0.8784 | 0.6216 | 0.4947 | | | | |
| 4 | 1.2946 | 1.2116 | 1.3003 | 1.2216 | 1.1657 | 1.0251 | 0.8785 | 0.5810 | | | |
| 5 | 1.1433 | 1.3655 | 1.2543 | 1.3806 | 1.2271 | 1.2508 | 1.0286 | 0.8784 | 0.5005 | | |
| 6 | 1.3100 | 1.2464 | 1.3974 | 1.3081 | 1.3921 | 1.2571 | 1.2519 | 1.0276 | 0.6204 | | |
| 7 | 1.1117 | 1.3287 | 1.2444 | 1.4173 | 1.3214 | 1.3897 | 1.2264 | 1.1714 | 0.8825 | | |
| 8 | 1.2795 | 1.2129 | 1.3449 | 1.2976 | 1.4331 | 1.3215 | 1.3912 | 1.2337 | 1.0580 | 0.6008 | |
| 9 | 1.0992 | 1.2855 | 1.2149 | 1.3855 | 1.2950 | 1.4599 | 1.3022 | 1.3211 | 1.0658 | 0.8916 | 0.4661 |
| 10 | 1.2416 | 1.1151 | 1.2971 | 1.2563 | 1.3949 | 1.3121 | 1.4272 | 1.2295 | 1.2181 | 0.9630 | 0.5311 |
| 11 | 1.0606 | 1.2323 | 1.0996 | 1.3118 | 1.1530 | 1.3632 | 1.1793 | 1.3171 | 1.1215 | 1.0286 | 0.6848 |

**Figure 3-5. Relative Energy by Bundle at Core Midplane – Cycle 8**

| J= \ I= | 12 | 13 | 14 | 15 | 16 | 17 | 18 | 19 | 20 | 21 | 22 |
|---|---|---|---|---|---|---|---|---|---|---|---|
| 1 | 0.5522 | 0.4992 | 0.4695 | | | | | | | | |
| 2 | 1.0021 | 0.9568 | 0.8858 | 0.5942 | | | | | | | |
| 3 | 1.0513 | 1.2197 | 1.1594 | 1.0169 | 0.7151 | 0.5584 | 0.4364 | | | | |
| 4 | 1.3715 | 1.2677 | 1.3355 | 1.1509 | 1.1147 | 0.9061 | 0.8292 | 0.4728 | | | |
| 5 | 1.2968 | 1.5019 | 1.2777 | 1.3904 | 1.1216 | 1.2040 | 1.0027 | 0.8304 | 0.4441 | | |
| 6 | 1.5073 | 1.4201 | 1.5356 | 1.3419 | 1.4193 | 1.2044 | 1.2066 | 0.9100 | 0.5561 | | |
| 7 | 1.2536 | 1.4755 | 1.3241 | 1.5551 | 1.3167 | 1.4279 | 1.1302 | 1.1211 | 0.7144 | | |
| 8 | 1.3724 | 1.3422 | 1.4895 | 1.4338 | 1.5792 | 1.3611 | 1.4079 | 1.1620 | 1.0272 | 0.5960 | |
| 9 | 1.2138 | 1.4005 | 1.2386 | 1.5970 | 1.4492 | 1.5772 | 1.3281 | 1.3577 | 1.1766 | 0.8999 | 0.4779 |
| 10 | 1.3978 | 1.3069 | 1.4393 | 1.4812 | 1.6482 | 1.4817 | 1.5427 | 1.2988 | 1.2456 | 0.9741 | 0.5130 |
| 11 | 1.1135 | 1.3840 | 1.2353 | 1.5868 | 1.4585 | 1.6097 | 1.3698 | 1.4148 | 1.0801 | 1.0218 | 0.5671 |

# 4.0 FLUX RESULTS FOR CYCLES 9 AND 8

## 4.1 Neutron Flux at RPV Inside Surface

The calculated peak fast flux (E>1 MeV) at the RPV inside surface is 2.97E8 n/cm$^2$-s for Cycle 9 and 2.70E8 n/cm$^2$-s for Cycle 8. The azimuthal flux profile for the RPV is illustrated in Figure 4-1. The averaged flux values are based on the weighting of cycle specific EFPY - 1.14 EFPY for Cycle 9 and 0.76 EFPY for Cycle 8. The peak flux for the first quadrant is located at the azimuth of 0°. The effects of inelastic scattering by steel in the jet-pump components are clearly displayed in Figure 4-1, where the flux depression occurs in regions shadowed by metal components. The flux level at 90° is slightly lower than its mirror image at 0° due to the shadowing effect of the jet-pump riser at 90°. Fluxes for other quadrants are expected to be similar due to quadrant symmetry of the core design as well as the arrangement of vessel internal components.

Axial flux variation at the RPV inside surface is shown in Figure 4-2. The elevation of peak flux occurs at 92 and 96 inches above the BAF for Cycle 9 and Cycle 8, respectively. The ratio of peak flux to midplane (75 inches above the BAF) flux is 1.016 and 1.036, respectively.

## 4.2 Neutron Flux at Surveillance Capsule Location

[[

]]

## 4.3 Neutron Flux at Shroud Inside Surface

The calculated peak fast flux (E>1 MeV) at the shroud inside surface (nominal ID of 163.75 inches) is 8.38E10 n/cm$^2$-s for Cycle 9 and 7.78E10 n/cm$^2$-s for Cycle 8. The azimuthal flux profile for the first quadrant of the shroud is illustrated in Figure 4-3. The peak flux is located at the azimuth of 90° for Cycle 9 and 83° for Cycle 8. The variation of the peak azimuth is due to the core layout for the ENVY plant and the relative bundle power for the governing peripheral bundles. In fact, peak azimuth for the shroud is not distinctly defined as the flux variation in the range of 0° - 10° and 80° - 90° is less than 4% . Flux distributions for the other three quadrants are expected to be similar due to quadrant symmetry of the core design.

Axial flux variation at the shroud inside surface is shown in Figure 4-4. The elevation of peak flux occurs at 98 and 102 inches above the BAF for Cycle 9 and Cycle 8, respectively. The ratio of peak flux to midplane flux is 1.028 and 1.055, respectively.

### 4.4 Neutron Flux Summary

A summary of fast fluxes, including the peak flux at the 1/4T and 3/4T of the RPV, is shown in Tables 4-1 and 4-2. Also included is a comparison with the previous results from the Battelle calculation [7]. The 1/4T and 3/4T fluxes are results from flux calculations and not derived values based on Reg Guide 1.99 and are presented for comparison purpose only. The calculation uncertainty and bias of the 1/4T and 3/4T fluxes have not been assessed. [[

]] the measured flux of 1.80E8±0.14E8 n/cm$^2$-s (2σ uncertainty), with a [[ ]] The peak RPV flux of 2.86E8 n/cm$^2$-s is significantly higher than the Battelle calculation of 2.18E8 n/cm$^2$-s. The following are possible explanations for this difference:

1. The mesh size used in the GE calculation is significantly finer than the Battelle model.
2. Battelle calculation was based on the integrated power of Cycle 1 through Cycle 9, while GE calculation was based on Cycles 8 and 9 only.
3. GE uses ENDF/B-VI cross sections, while Battelle calculation was based on the cross section data from the early 1980s.

**Table 4-1 Comparison of RPV Flux and Shroud Flux - Cycles 9 and 8**

| | Battelle Calculation | Cycle 9 | Cycle 8 | C8-C9 Avg. |
|---|---|---|---|---|
| Peak RPV Flux (>1 MeV) | | | | |
| Inside Surface | 2.18E8 | 2.97E8 | 2.70E8 | 2.86E8 |
| 1/4T | 1.59E8 | 2.05E8 | 1.87E8 | 1.98E8 |
| 3/4T | 6.23E7 | 8.57E7 | 7.80E7 | 8.26E7 |
| | | | | |
| Peak Shroud Flux | | 8.38E+10 | 7.78E+10 | 8.11E+10 |

**Table 4-2 Comparison of 30° Capsule Flux**

| | Battelle Measured Flux (±2σ) | GE* | GE – Battelle Difference |
|---|---|---|---|
| Fast Flux (> 1 MeV) | 1.80E8±0.14E8 | [[ | ]] |

* [[

]]

**Figure 4-1. Azimuthal Distribution of Fast Neutron Flux at RPV Inside Surface at Peak Elevation – Cycles 9 and 8**

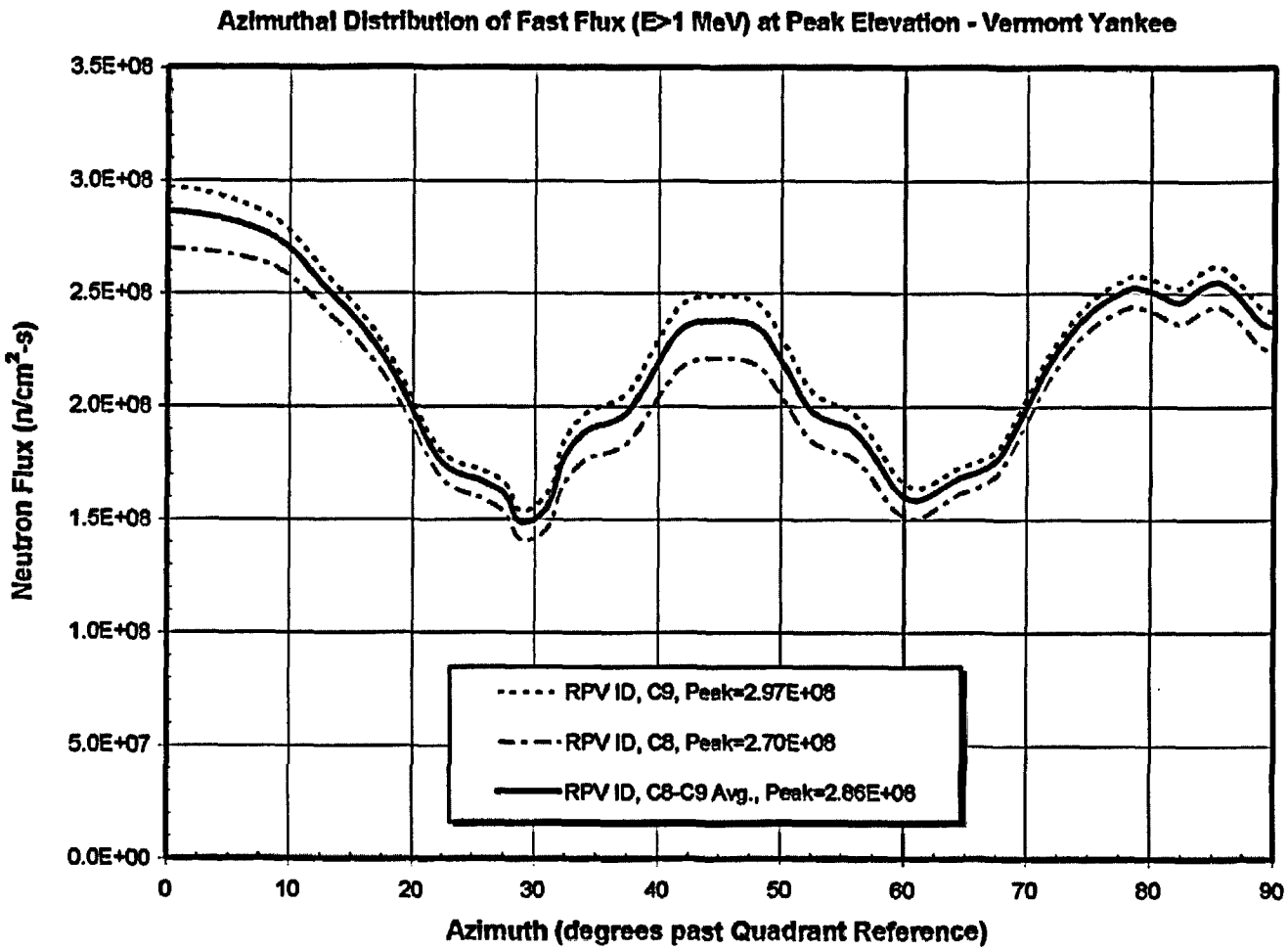

**Figure 4-2. Axial Distribution of Fast Neutron Flux at RPV Inside Surface – Cycles 9 and 8**

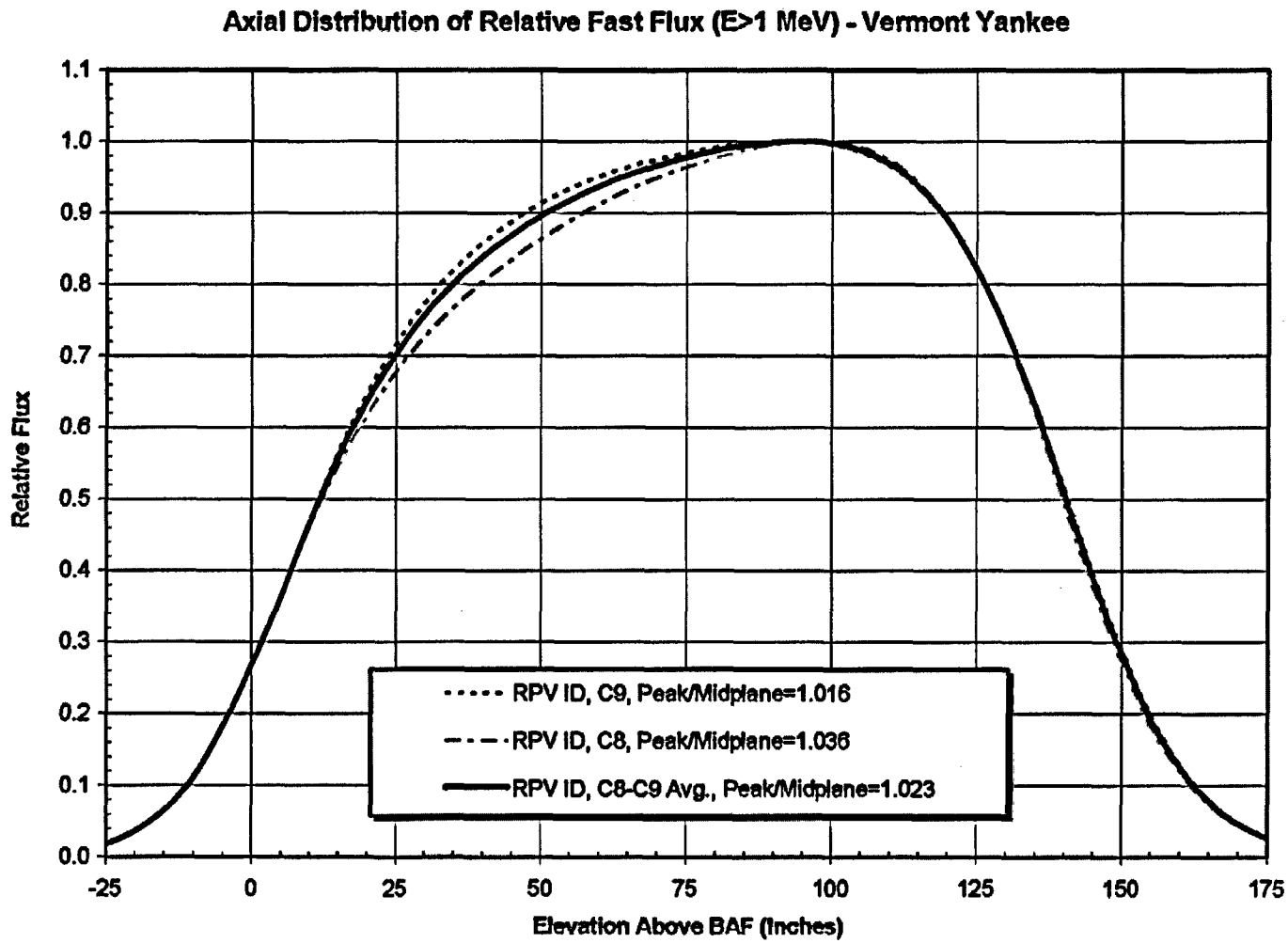

**Figure 4-3. Azimuthal Distribution of Fast Neutron Flux at Shroud Inside Surface at Peak Elevation – Cycles 9 and 8**

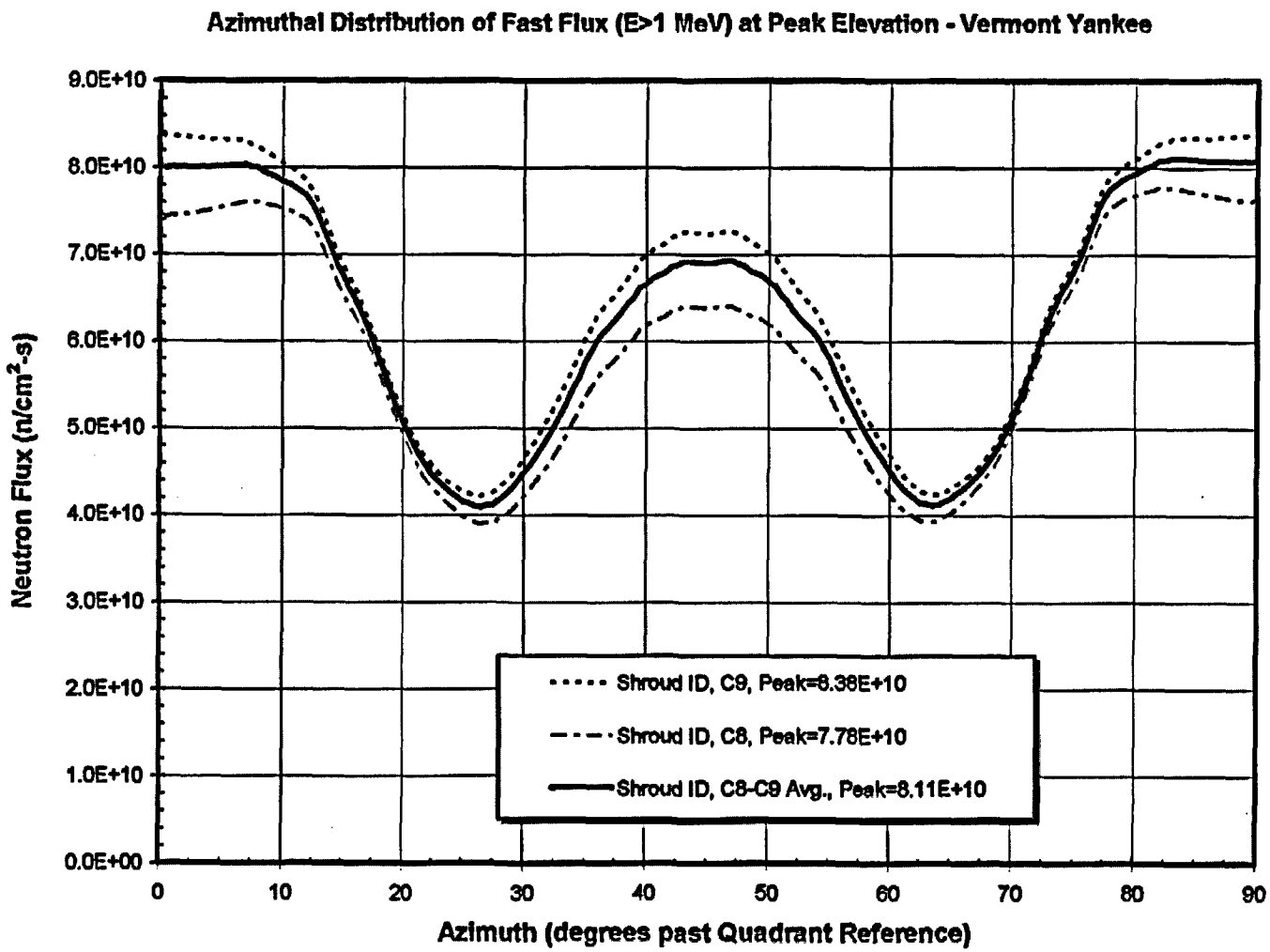

**Figure 4-4. Axial Distribution of Fast Neutron Flux at Shroud Inside Surface – Cycles 9 and 8**

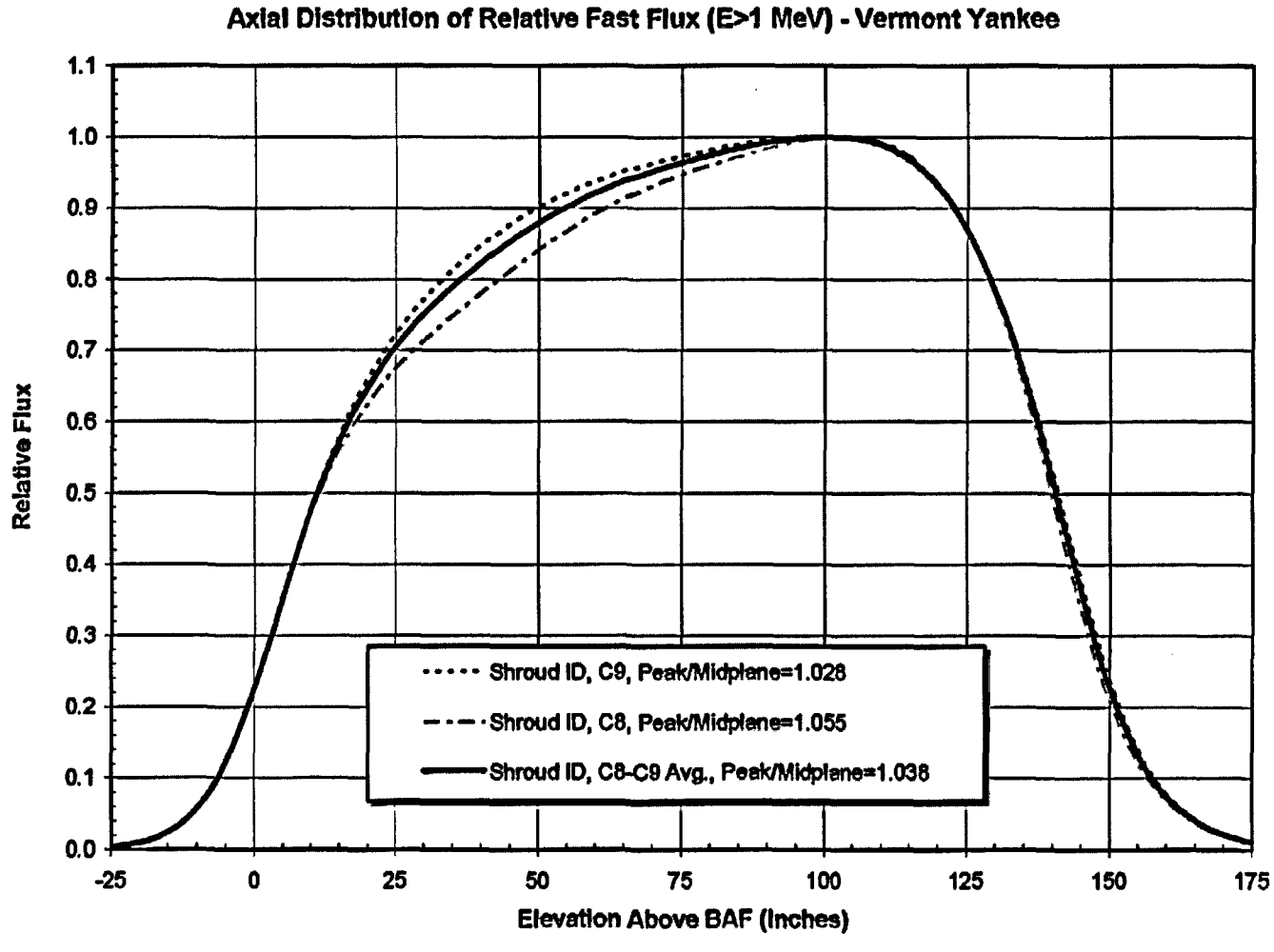

## 5.0 FLUX RESULTS FOR MODERN CORES

Cycle 21 has been selected as a representative cycle for the modern core design. The selection of Cycle 21 to represent the modern cores, as agreed by ENVY as part of the Design Input Request, was based on a review of the core design data of a number of recent cycles, which concluded that Cycle 21 flux would bound the average of the modern cores. Flux results for Cycle 21 are documented in this section. The flux results for the average of Cycles 9 and 8 are also shown for a one-on-one comparison. An assessment of Cycle 23, which contains fuel bundles with part-length rods in the core periphery, is also presented here.

### 5.1 Neutron Flux at RPV Inside Surface

The calculated peak fast flux (E>1 MeV) at the RPV inside surface is 2.96E8 n/cm$^2$-s for Cycle 21. This flux value is nearly identical to that of Cycle 9. The azimuthal flux profile for the RPV is illustrated in Figure 5-1 for the cases with and without the tie rods included in the model. The peak flux for the first quadrant is located at the azimuth of 0°. The flux level at 90° is slightly lower than that at 0° due to the shadowing effect of the jet-pump riser at 90°. The effect of the shroud restraint tie rods at the 45° azimuth in this quadrant, which were installed during 1996, is clearly shown in Figure 5-1. The flux depression is maximized at about 25% at 45° and then gradually reduced to insignificant amount beyond the range of 40° - 60°.

Axial flux variation at the RPV inside surface is shown in Figure 5-2. The elevation of peak flux occurs at 84 inches above the BAF. The ratio of peak flux to midplane (75 inches above BAF) flux is 1.008.

### 5.2 Neutron Flux at Surveillance Capsule Location

[[

]]

### 5.3 Neutron Flux at Shroud Inside Surface

The calculated peak fast flux (E>1 MeV) at the shroud inside surface is 8.17E10 n/cm$^2$-s for Cycle 21. The azimuthal flux profile for the first quadrant of the shroud is illustrated in Figure 5-3. The peak flux for the first quadrant is located at the azimuth of 83°.

Flux distributions for the other three quadrants are expected to be similar due to quadrant symmetry of the core design.

Axial flux variation at the shroud inside surface is shown in Figure 5-4. The elevation of peak flux occurs at 89 inches above the BAF. The ratio of peak flux to midplane flux is 1.014.

### 5.4 Neutron Flux Summary

A summary of fast fluxes, including the peak flux at the 1/4T and 3/4T of the RPV, is shown in Table 5-1. Also included is a comparison with the previous results from the Battelle calculation and the averaged values of Cycles 9 and 8. As stated in Section 4.4, the 1/4T and 3/4T fluxes are results from flux calculations and not derived based on Reg Guide 1.99 and are presented for comparison purpose only. The calculation uncertainty and bias of these data have not been assessed. These results show that Cycle 21 fluxes are comparable to those of the averaged values of Cycles 9 and 8, [[

]] This implies that Cycle 21 fluxes can be used to represent older cycles for the purpose of estimating the life-time neutron fluences. The results imply that the Cycle 21 peak flux is acceptable for representing older cycles.

**Table 5-1 Summary of Flux Results – Cycle 21**

| | Battelle Calculation | C8-C9 Avg. | Cycle 21 |
|---|---|---|---|
| Peak RPV Flux (>1 MeV) | | | |
| Inside Surface | 2.18E8 | 2.86E8 | 2.96E8 |
| 1/4T | 1.59E8 | 1.98E8 | 2.05E8 |
| 3/4T | 6.23E7 | 8.26E7 | 8.56E7 |
| Capsule | | | |
| Fast Flux | 1.80E8 | [[ ]] | [[ ]] |
| Calculated/Measured* | | [[ ]] | [[ ]] |
| Lead Factor | 0.83 | [[ ]] | [[ ]] |
| | | | |
| Peak Shroud Flux | | 8.11E+10 | 8.17E+10 |

* Measured flux is 1.80E8

## 5.5 Assessment of Cycle 23

A simplified evaluation is performed to assess the effect of part-length rods on the RPV flux. The core load for Cycle 23 contains fuel bundles with part-length rods in the core periphery that might impact the RPV flux level. Based on the Reference Loading Pattern (RLP) core design data for Cycle 23 provided by the Global Nuclear Fuel (GNF), one can derive the nodal power/energy distribution using the procedure described in Section 3.3.5. Study of bundle importance function, that is applicable to the ENVY plant, indicates that the peak flux for the RPV and shroud wall is dominated by a few peripheral bundles that are closest to the peak azimuth. [[

]] (see Figure 3-1 for bundle identification). Comparison of power distribution of these [[ ]] bundles between Cycle 21 and Cycle 23 provides indication of relative flux levels. Figure 5-5 shows a comparison of the axial nodal distribution of cycle energy for the average of these [[ ]] dominant bundles. Figure 5-6 shows the bundle-dependent relative cycle energy (normalized to the core average) at core midplane elevation for Cycle 23.

The axial average of relative nodal energy in the [[ ]] dominant peripheral bundles is 0.34 for Cycle 23 and 0.45 for Cycle 21. Similarly, the midplane relative energy in the [[ ]] dominant peripheral bundles is 0.43 for Cycle 23 and 0.56 for Cycle 21. Therefore, the peak vessel and shroud fluxes for Cycle 23 will be bounded by Cycle 21 due to the significantly lower power in these bundles for Cycle 23.

[[

]]

**Figure 5-1. Azimuthal Distribution of Fast Neutron Flux at RPV Inside Surface at Peak Elevation – Cycle 21**

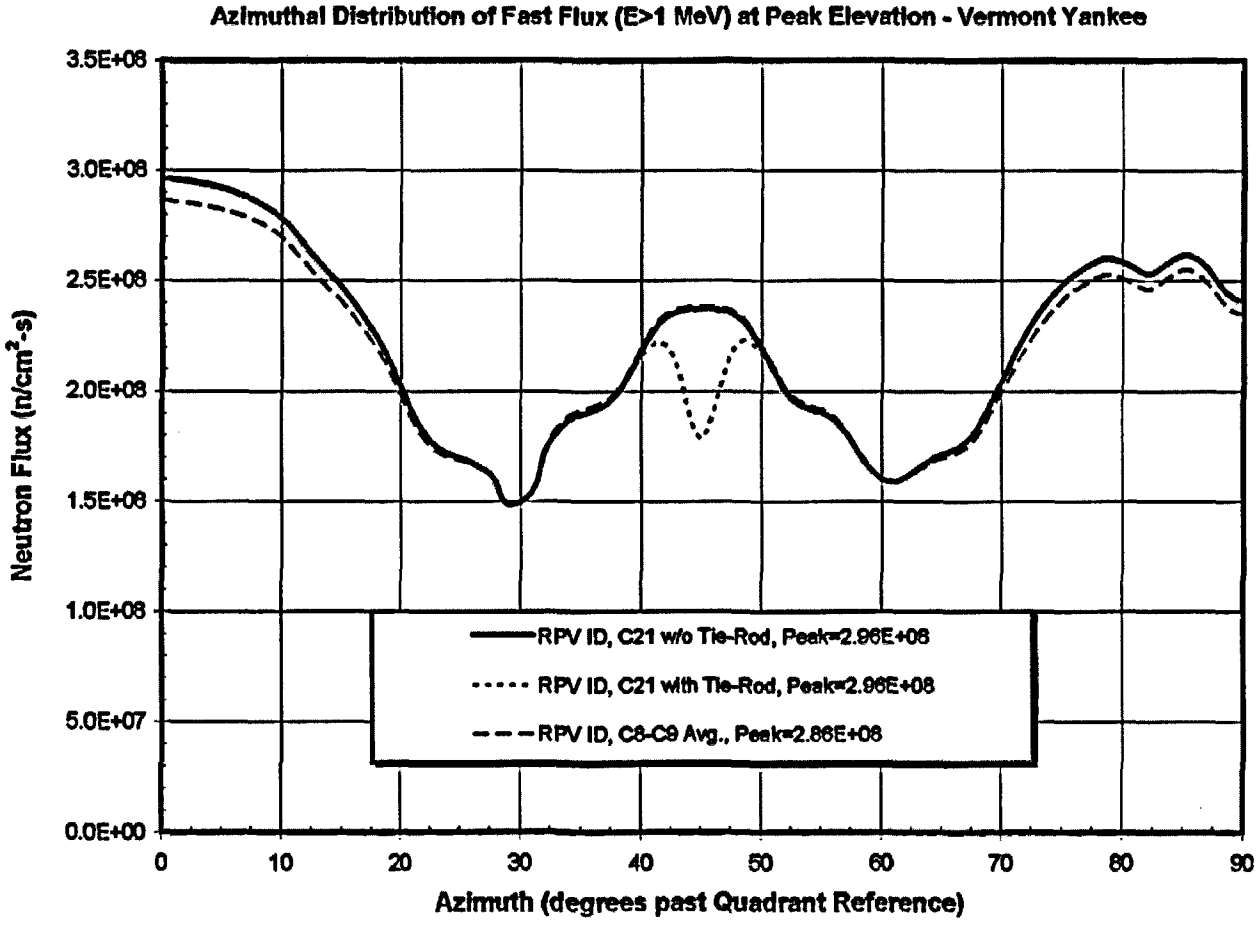

**Figure 5-2. Axial Distribution of Fast Neutron Flux at RPV Inside Surface – Cycle 21**

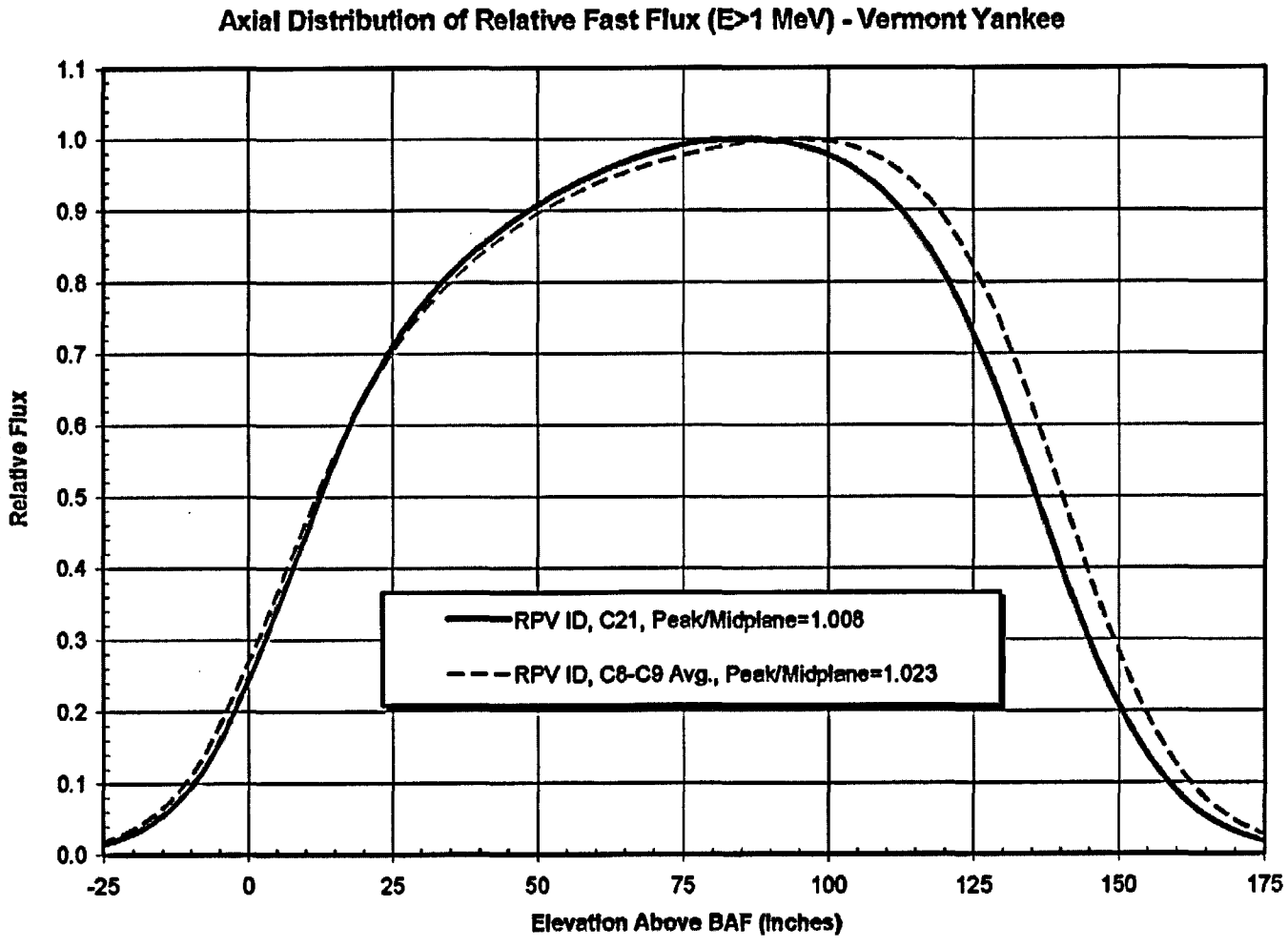

**Figure 5-3. Azimuthal Distribution of Fast Neutron Flux at Shroud Inside Surface at Peak Elevation – Cycle 21**

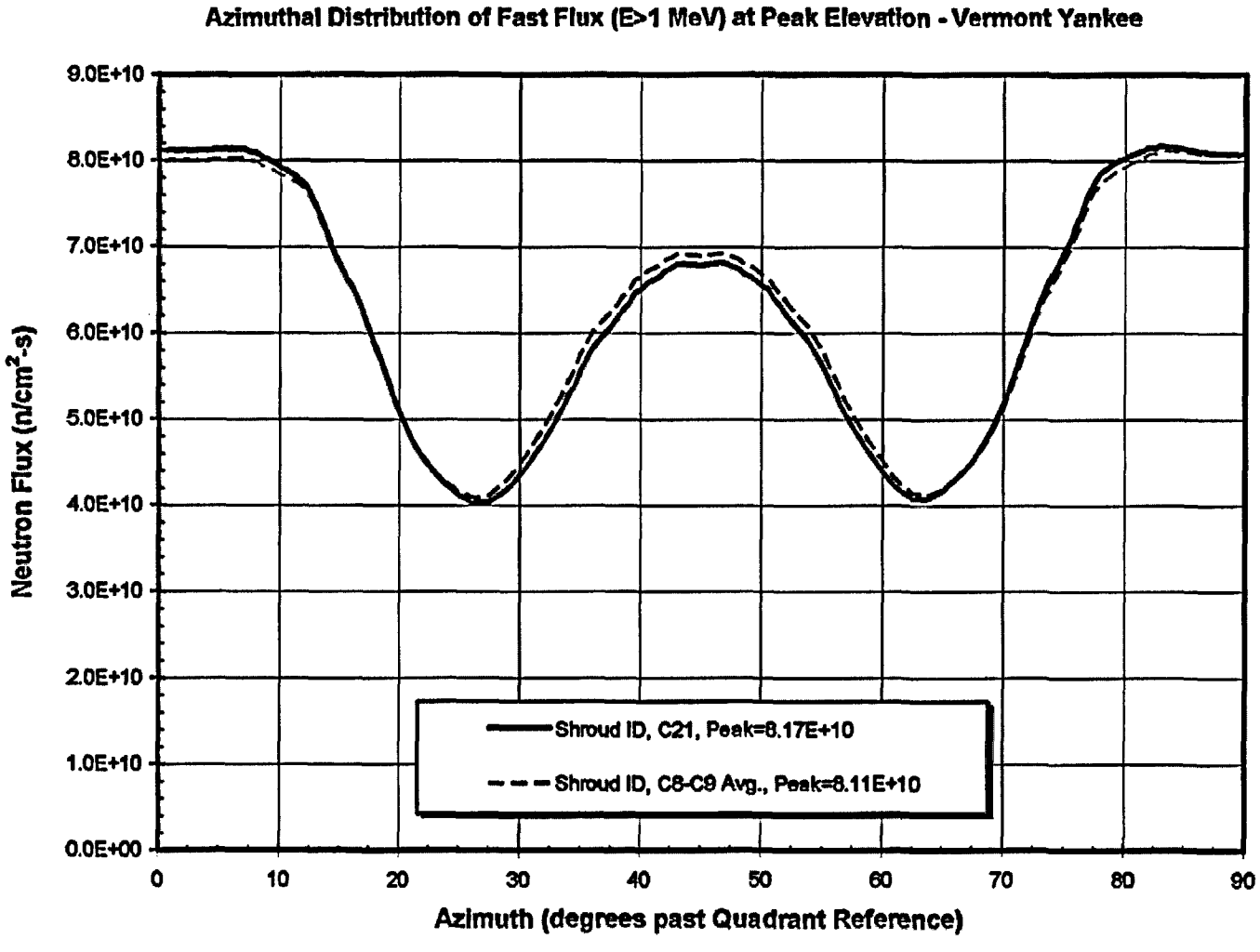

**Figure 5-4. Axial Distribution of Fast Neutron Flux at Shroud Inside Surface – Cycle 21**

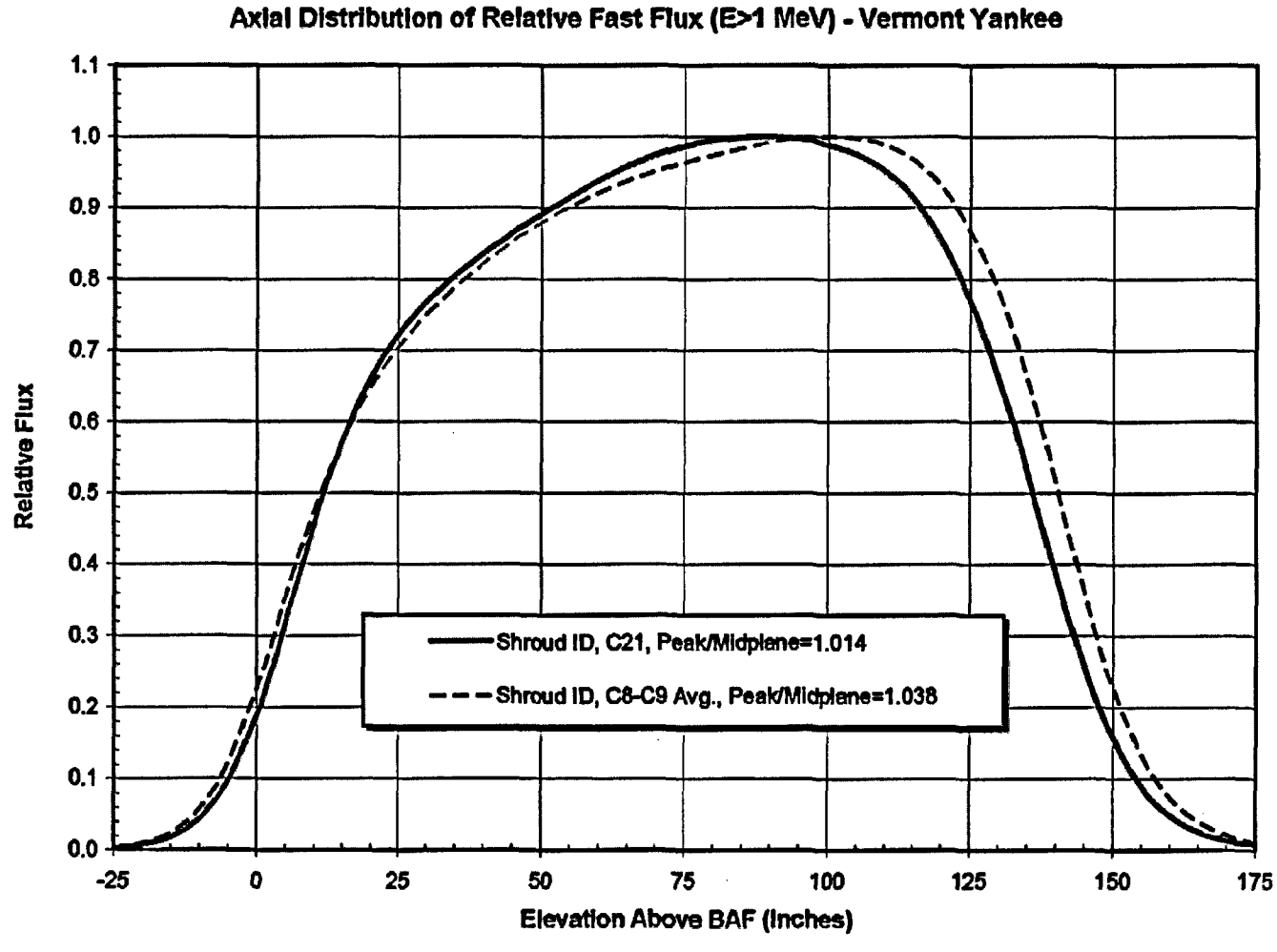

**Figure 5-5. Axial Power Profiles of the Dominant Bundles**

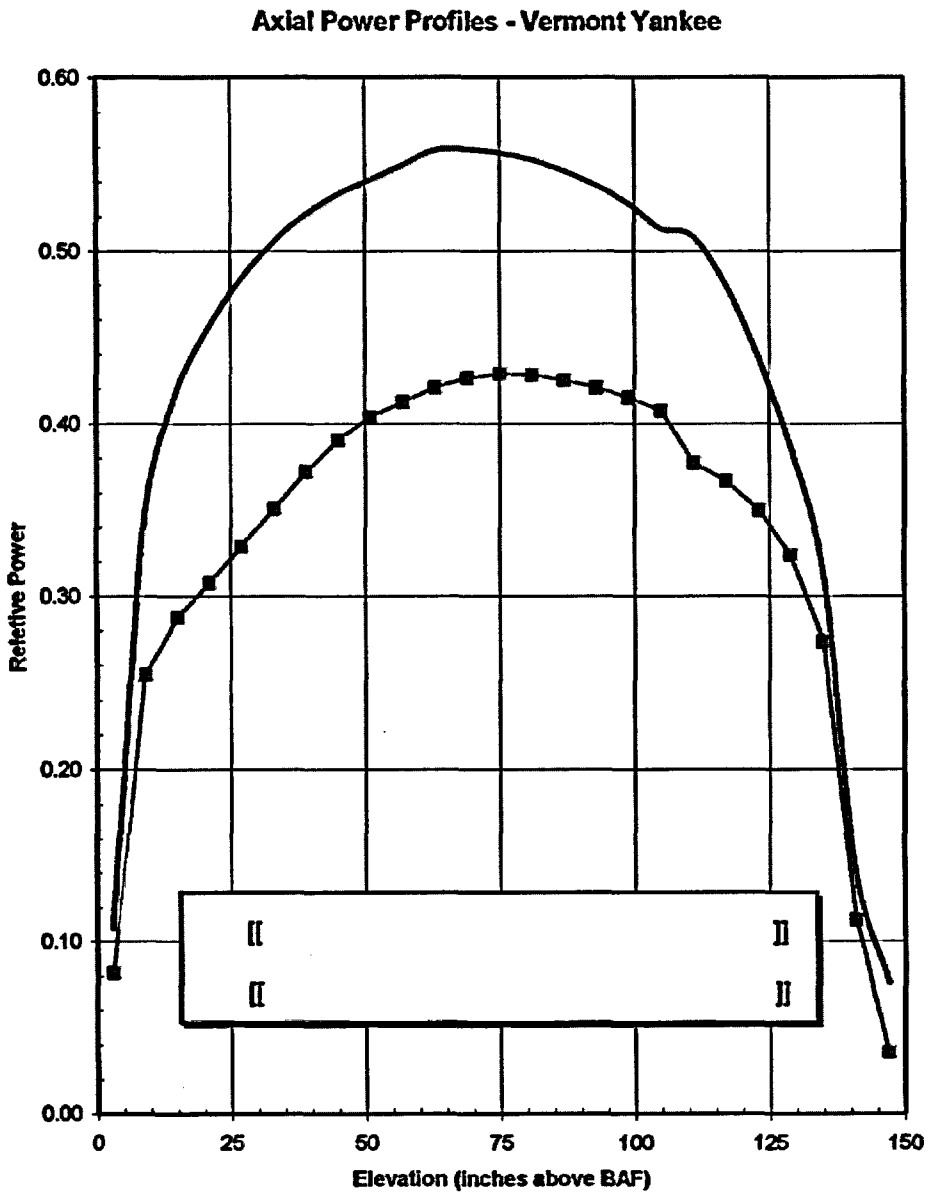

**Figure 5-6. Relative Energy by Bundle at Core Midplane – Cycle 23**

| J= \ I= | 12 | 13 | 14 | 15 | 16 | 17 | 18 | 19 | 20 | 21 | 22 |
|---|---|---|---|---|---|---|---|---|---|---|---|
| 1 | 0.4938 | 0.4528 | 0.3392 | | | | | | | | |
| 2 | 1.0690 | 1.0152 | 0.6705 | 0.4512 | | | | | | | |
| 3 | 1.3543 | 1.2456 | 1.2567 | 0.7872 | 0.6526 | 0.5115 | 0.3367 | | | | |
| 4 | 1.0259 | 1.5231 | 1.3691 | 1.4171 | 1.1939 | 1.0509 | 0.6270 | 0.4038 | | | |
| 5 | 1.5750 | 1.4965 | 1.6358 | 1.4476 | 1.4812 | 1.2252 | 1.1390 | 0.6374 | 0.3375 | | |
| 6 | 1.1147 | 1.6821 | 1.1773 | 1.6662 | 1.1081 | 1.4499 | 1.2208 | 1.0496 | 0.5123 | | |
| 7 | 1.7377 | 1.5666 | 1.7179 | 1.5703 | 1.6797 | 1.1050 | 1.4793 | 1.1864 | 0.6524 | | |
| 8 | 1.4692 | 1.7118 | 1.1767 | 1.7148 | 1.5575 | 1.6604 | 1.4509 | 1.4202 | 0.7902 | 0.4535 | |
| 9 | 1.6589 | 1.1418 | 1.6063 | 1.1275 | 1.6604 | 1.1675 | 1.6434 | 1.3800 | 1.2666 | 0.6753 | 0.3428 |
| 10 | 1.3284 | 1.5939 | 1.1253 | 1.6474 | 1.5077 | 1.6894 | 1.5199 | 1.5481 | 1.2611 | 1.0254 | 0.4579 |
| 11 | 1.0113 | 1.3177 | 1.6382 | 1.4461 | 1.7330 | 1.1772 | 1.6654 | 1.0602 | 1.3803 | 1.0845 | 0.5014 |

## 6.0 NEUTRON FLUENCE

A conservative estimation of fast neutron fluences at the end of plant life of 32 and 54 EFPY can be obtained by multiplying the neutron fluxes with the EFPY. For Entergy Northeast Vermont Yankee, the bounding peak RPV flux is 2.96E8 n/cm$^2$-s. The bounding peak shroud flux is 8.17E10 n/cm$^2$-s. [[ ]]
Based on these flux values, the 32-EFPY and 54-EFPY fluences are calculated, as summarized below:

| | Peak RPV | Capsule | | Peak Shroud |
|---|---|---|---|---|
| Fast Flux, n/cm$^2$-s | 2.96E8 | [[ | ]] | 8.17E10 |
| 32-EFPY Fluence, n/cm$^2$ | 2.99E17 | [[ | ]] | 8.25E19 |
| 54-EFPY Fluence, n/cm$^2$ | 5.04E17 | [[ | ]] | 1.39E20 |

Figure 6-1 shows the axial distribution of 32-EFPY fast neutron fluence at the peak azimuth of the RPV inside surface. The results of the analysis demonstrate the fast fluence outside the active axial fuel zone at the RPV is less than 1.0E17 n/cm$^2$. This conclusion is depicted in Figure 6-1.

**Figure 6-1. Axial Distribution of 32-EFPY Fast Neutron Fluence at RPV Inside Surface**

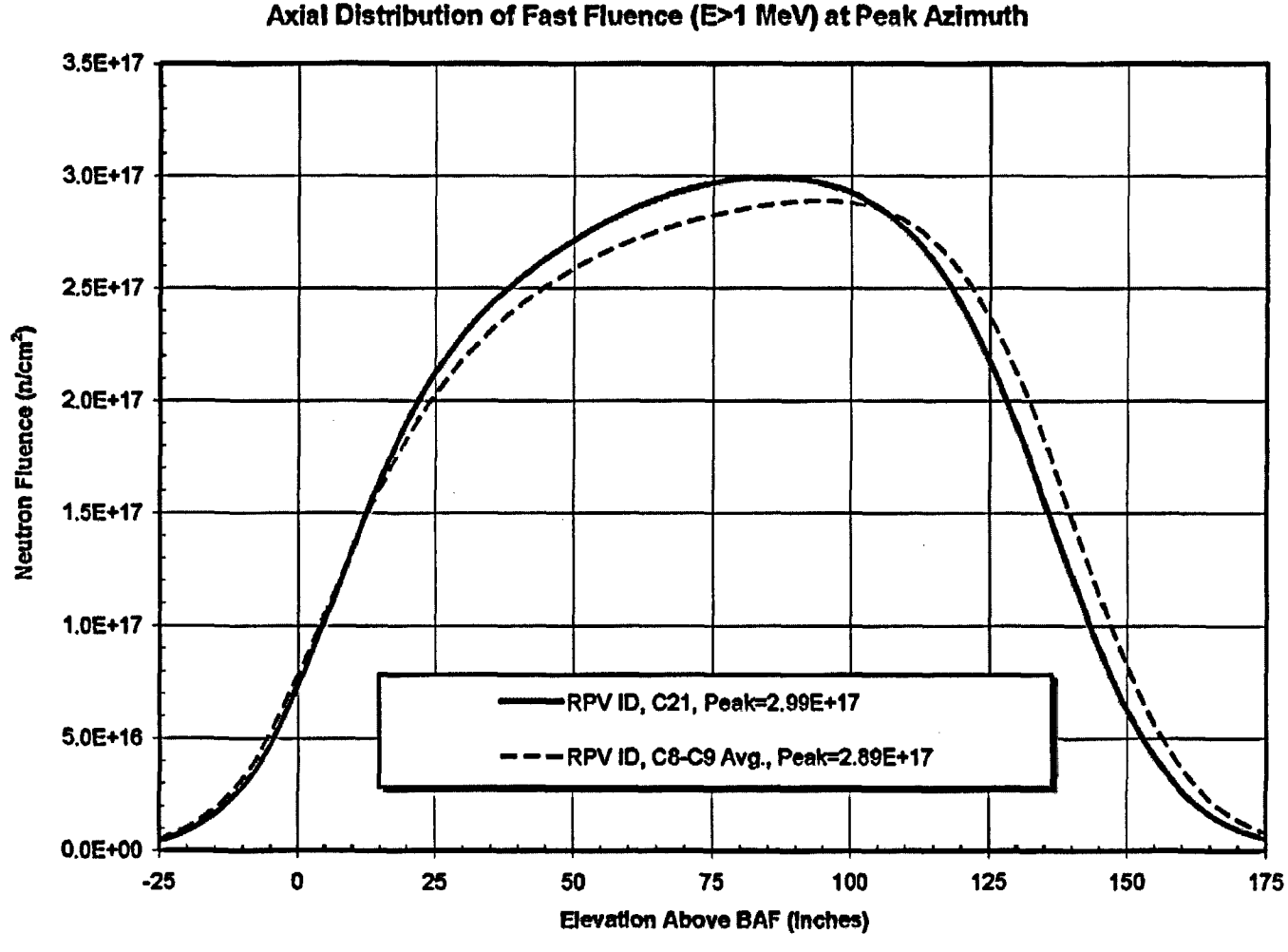

## 7.0 REFERENCES


1. NEDC-32983P-A, Rev. 1, "Licensing Topical Report, General Electric Methodology for Reactor Pressure Vessel Fast Neutron Flux Evaluations," December 2001.
2. Letter, S. A. Richards (USNRC) to J. F. Klapproth, "Safety Evaluation for NEDC-32983P, General Electric Methodology for Reactor Pressure Vessel Fast Neutron Flux Evaluation (TAC No. MA9891)," MFN 01-050, September 14, 2001.
3. Regulatory Guide 1.190, "Calculational and Dosimetry Methods for Determining Pressure Vessel Neutron Fluence," U.S. NRC, March 2001.
4. CCC-543, "TORT-DORT Two- and Three-Dimensional Discrete Ordinates Transport Version 2.8.14," Radiation Shielding Information Center (RSIC), January 1994.
5. "VY Fluence Evaluation Input Request from GE," Technical Evaluation No. TE-2002-031, Rev. 2, dated 10/2/2002.
6. R. J. Weader II to P. Perez and T. Wu, "VY Cycles 8 and 9 Fluence Calculation Data," Entergy Memo NEA-02-246, January 8, 2003.
7. BCL-585-84-3, "Examination, Testing and Evaluation of Irradiated Pressure Vessel Surveillance Specimens from the Vermont Yankee Nuclear Power Station," Battelle Columbus Laboratories, May 15, 1984.
8. Letter, S. A. Richards (USNRC) to G. A. Watford, "Amendment 26 to GE Licensing Topical Report NEDE-24011-P-A, GESTAR II – Implementing Improved GE Steady-State Methods (TAC No. MA6481)," November 10, 1999.
9. T Wu and H. A. Careway, "Discrete Ordinates Code Package User's Manual," November, 2001.